Role of the higher static deformations of fragments in the cold binary fission of ^{252}Cf

A. Săndulescu,[1,2,3] Ş. Mişicu,[1] F. Cârstoiu,[1] A. Florescu,[1,2] and W. Greiner[2,3]
[1]*Institute of Atomic Physics, Bucharest, P.O. Box MG-6, Romania*
[2]*Physics Department, Vanderbilt University, Nashville, Tennessee 37235*
[3]*Institut für Theoretische Physik der J.W.Goethe Universität, D-60054, Frankfurt am Main, Germany*
(Received 18 December 1997)

We study the binary cold fission of ^{252}Cf in the frame of a cluster model where the fragments are born to their respective ground states and interact via a double-folded potential with deformation effects taken into account up to multipolarity $\lambda=4$. The preformation factors were neglected. In the case when the fragments are assumed to be spherical or with ground-state quadrupole deformation, the Q-value principle dictates the occurrence of a narrow region around the double magic ^{132}Sn, like in the case of cluster radioactivity. When the hexadecupole deformation is turned on, an entire mass region of cold fission in the range 138–156 for the heavy fragment arise, in agreement with the experimental observations. This fact suggests that in the above-mentioned mass region, contrary to the usual cluster radioactivity where the daughter nucleus is always a neutron/proton (or both) closed shell or nearly closed shell spherical nucleus, the clusterization mechanism seems to be strongly influenced by the hexadecupole deformations rather than the Q value. [S0556-2813(98)05705-7]

PACS number(s): 25.85.Ca, 21.60.Gx, 23.70.+j, 27.90.+b

I. INTRODUCTION

In the binary nuclear fission of actinide nuclei the fragments are usually formed in highly excited states which subsequently decay to their ground states by emitting neutrons and γ rays. However a small fraction of these fragmentations will attain a very high kinetic energy TKE which is very close to the corresponding binary decay energy Q. Since in this case the fragments are formed with excitation energies close to their ground states no neutrons are emitted. Milton and Fraser [1] noticed that some of the fission fragments are produced at such high kinetic energies that the emerging nuclei are formed nearly in their ground state. Later on Guet *et al.* [2] confirmed the previous interpretation by determining the mass distributions of the primary fragments for the highest values of the kinetic energy. They concluded that even before the scission takes place we deal with a superposition of two fragments in their ground state, from which the *cold fragmentation* term emerged. An interesting remark they made was that the odd-even fluctuations of Q due to nucleon pairing were not present also in the $TKE_{\max}$ values. In their view this smoothing of the odd-even effect was a consequence of a pair broken from one of the fragments. The probability for neutronless fission is 0.0021 ± 0.0008 for ^{252}Cf.

In the last years the cold (neutronless) fission of many actinide nuclei into fragments with masses from ≈ 70 to $\approx$ 160 was an intensively studied phenomenon [3–9]. An important step in the understanding of the cold fission phenomenon was the observation that the final nuclei are generated in their ground states or some low excited states, which prompted some authors to relate these decays to the spontaneous emission of light nuclei (cluster radioactivity) such as α particles and heavier clusters ranging from ^{14}C to ^{34}Si [10].

The fragments emitted in binary cold decays are produced with very low or even zero internal excitation energy and consequently with very high kinetic energy $TKE=Q-TXE$. In order to achieve such large TKE values, both fragments should have very compact shapes at the scission point and deformations close to those of their ground states [3,11].

The first direct observation of cold (neutronless) binary fragmentations in the spontaneous fission of ^{252}Cf was made by using the multiple Ge-detector Compact Ball facility at Oak Ridge National Laboratory [7,8], and more recently with the Gammasphere consisting of 72 detectors [9]. Using the triple-gamma coincidence technique, the correlations between the two fragments were observed unambiguously. In these cold fragmentations, some indications of a third light fragment such as α, ^{6}He and ^{10}Be clusters [12–14], were also reported.

In a recent series of publications [15,16] the Tübingen group reported some interesting results on the spontaneous decay of ^{252}Cf using a twin ionization chamber. Two distinct mass regions of cold fission were observed: the first extending from the mass split 96/156 up to 114/138 and the second one comprising only a narrow mass range around the mass split 120/132.

In the present paper, based on a cluster model similar to the cluster model used for cluster radioactivity, we estimated the relative isotopic yields for the spontaneous cold binary fission of ^{252}Cf. These isotopic yields are given by the ratio of the penetrability through the potential barrier between the two final fragments for a given mass and charge splitting, over the sum of penetrabilities for all possible fragmentations.

The corresponding barriers were evaluated using the double folding potential with $M3Y$ nucleon-nucleon effective interactions and realistic ground-state deformations including the octupole and hexadecupole ones [13]. We were mainly concerned with the study of the influence of the fragment deformations on the yields and we concluded that the occurence of the two mass regions of cold fission is deter-

mined essentially by the ground-state hexadecupole deformations.

II. DEFORMATION-DEPENDENT CLUSTER MODEL

In the present paper we consider a deformation-dependent cluster model, similar to the one-body model used for the description of cluster radioactivity [10]. The initial nucleus is assumed to be already separated into two parts, a heavy one and a light cluster, and the preformation factors for the fragments are not taken into account. An advantage of this model is that the barrier between the two fragments can be calculated quite accurately due to the fact that the touching configurations are situated inside of the barriers. The Q values and the deformation parameters contain all nuclear shell and pairing effects of the corresponding fragments.

The barriers were calculated using the double folding model for the heavy-ion interaction

$$V_F(\mathbf{R})=\int d\mathbf{r}_1 d\mathbf{r}_2 \rho_1(\mathbf{r}_1)\rho_2(\mathbf{r}_2)v(\mathbf{s}), \tag{1}$$

where $\rho_{1(2)}(\mathbf{r})$ are the ground-state one-body densities of the fragments and v is the NN effective interaction. The separation distance between two interacting nucleons is denoted by $\mathbf{s}=\mathbf{r}_1+\mathbf{R}-\mathbf{r}_2$, where R is the distance between the c.m. of the two fragments. We have chosen the G-matrix $M3Y$ effective interaction which is representative for the so-called local and density-independent effective interactions [17]. This interaction is particularly simple to use in folding models since it is parametrized as a sum of three Yukawa functions in each spin-isospin (S,T) channel. In the present study the spin and spin-isospin-dependent components have been neglected since for a lot of fragments involved in the calculation the ground-state spins are unknown. The spin-spin component of the heavy-ion potential can be neglected here since it is of the order $1/A_1A_2$. Only the isoscalar and isovector components have been retained in the present study for the central heavy-ion interaction.

The $M3Y$ interaction is dominated by the one-nucleon knock-on exchange term, which leads to a nonlocal kernel. In the present case the nonlocal potential is reduced to a zero range pseudopotential $\hat{J}_{00}\delta(\mathbf{s})$, with a strength depending slightly on the energy. We have used the common prescription [17] $\hat{J}_{00}=-276$ MeV fm^3 neglecting completely the small energy dependence. For example, the odd-even staggering in the Q value for a fragmentation channel, which is typically of the order $\Delta Q=2$ MeV, leads to a variation with $\Delta\hat{J}_{00}=-0.005\ (\Delta Q/\mu)$ MeV fm^3 with $\mu\approx 100$. The one-body densities in Eq. (1) are taken as Fermi distributions in the intrinsic frame

$$\rho(\mathbf{r})=\frac{\rho_0}{1+e^{(r-c)/a}} \tag{2}$$

with $c=c_0[1+\Sigma_{\lambda\geq 2}\beta_\lambda Y_{\lambda 0}(\Omega)]$. Only static axial symmetric deformations are considered. The half radius c_0 and the diffusivity a are taken from the liquid drop model (LDM) [18]. The normalization constant ρ_0 is determined by requiring the particle number conservation

$$\int r^2 dr\, d\Omega \rho(r,\Omega)=A \tag{3}$$

and then the multipoles are computed numerically

$$\rho_\lambda(r)=\int d\Omega \rho(r,\Omega)Y_{\lambda 0}(\Omega). \tag{4}$$

Once the multipole expansion of the density is obtained, the integral in Eq. (1) becomes

$$V_F(\mathbf{R},\omega_1,\omega_2)=\sum_{\lambda_1\mu_1\lambda_2\mu_2} D^{\lambda_1}_{\mu_1 0}(\omega_1)D^{\lambda_2}_{\mu_2 0}(\omega_2)I_{\lambda_1\mu_1\lambda_2\mu_2}, \tag{5}$$

where [19]

$$I_{\lambda_1\mu_1\lambda_2\mu_2}=\sum_{\lambda_3\mu_3} B^{\lambda_3\mu_3}_{\lambda_1\mu_1\lambda_2\mu_2}\int r_1^2 dr_1 r_2^2 dr_2 \rho_{\lambda_1}(r_1)\rho_{\lambda_2}(r_2) \times F^v_{\lambda_1\lambda_2\lambda_3}(r_1,r_2,R) \tag{6}$$

and

$$F^v_{\lambda_1\lambda_2\lambda_3}(r_1,r_2,R)=\int q^2 dq \tilde{v}(q) j_{\lambda_1}(qr_1)j_{\lambda_2}(qr_2)j_{\lambda_3}(qr_3). \tag{7}$$

Above, $D^\lambda_{\mu 0}(\omega)$ stands for the Wigner rotation matrix describing the orientation ω of the intrinsic symmetry axis with respect to the fixed frame, $\tilde{v}(q)$ denotes the Fourier transform of the interaction and j_λ are the spherical Bessel functions. The matrix B in Eq. (6) is defined in [19] and contains selection rules for coupling angular momenta. Only $\lambda_1+\lambda_2+\lambda_3=$ even, are allowed. When $\beta_\lambda\neq 0$, $\lambda=2,3,4$ for both fragments, the sum in Eq. (5) involves 36 terms for a nose-to-nose configuration with $\lambda_3\leq 6$. For most of the fragmentation channels studied here, large quadrupole, hexadecupole, and occasionally octupole deformations are involved. Therefore a Taylor expansion method for obtaining the density multipoles turns out to be unsuitable. On the other hand, a large quadrupole deformation induces according to Eq. (4) nonvanishing multipoles with $\lambda=4$ and 6 even if $\beta_4=\beta_6=0$. Therefore for a correct calculation of Eq. (4), a numerical method with a truncation error of order $O(h^7)$ is needed in order to ensure the orthogonality of spherical harmonics with $\lambda\leq 6$. Performing the integrals (6) and (7) we have used a numerical method with a truncation error of the order $O(h^9)$. All short-range wavelength ($q\leq 10$ fm^{-1}) have been included and particular care has been taken to ensure the convergence of the integrals with respect to the integration step and the range of integration.

At the scission configuration two coaxial deformed fragments in contact at their tips were assumed. For quadrupole deformations we choose two coaxial prolate spheroids due to the fact that the prolate shapes are favored in fission. It is known that each oblate minimum always corresponds to another prolate minimum. For pear shapes, i.e., fragments with quadrupole and octupole deformations, we choose opposite signs for the octupole deformations, i.e., nose-to-nose configurations (see Fig. 1). For hexadecupole deformations we choose only positive signature, because it leads to a lowering

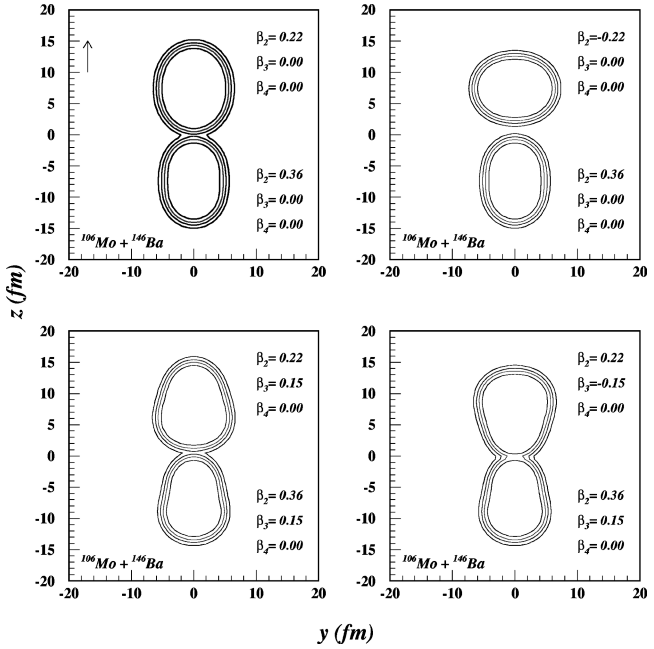

FIG. 1. Density plots of ^{106}Mo and ^{146}Ba fragments, placed at $R=15$ fm, considered with quadrupole and octupole deformations. In the upper part are represented the prolate-prolate, oblate-prolate positions and in the lower part two pear shapes nose to back and nose to nose. The positions are given by the deformation signs.

of the barriers in comparison with negative ones and consequently they are much more favored in fission (see Fig. 2).

In order to illustrate the influence of deformations on the barriers we displayed in Fig. 3 the $M3Y$-folding multipoles for ^{106}Mo and ^{146}Ba with all deformations included. The octupole component is large in the interior but gives negligible contribution in the barrier region in contrast to the

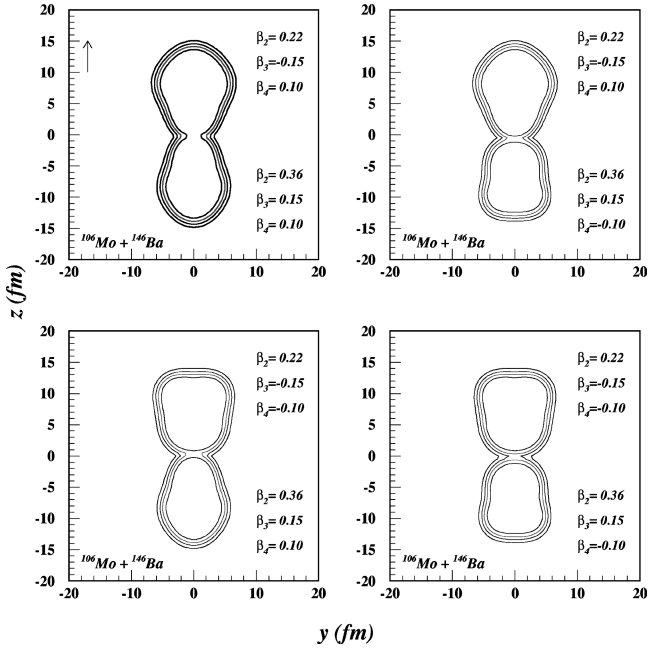

FIG. 2. Same as for Fig. 1. The influence of different signs of hexadecupole deformations on ^{106}Mo and ^{146}Ba densities in the presence of large quadrupole and octupole deformations. The penetrability is maximized for $\beta_4>0$ configurations.

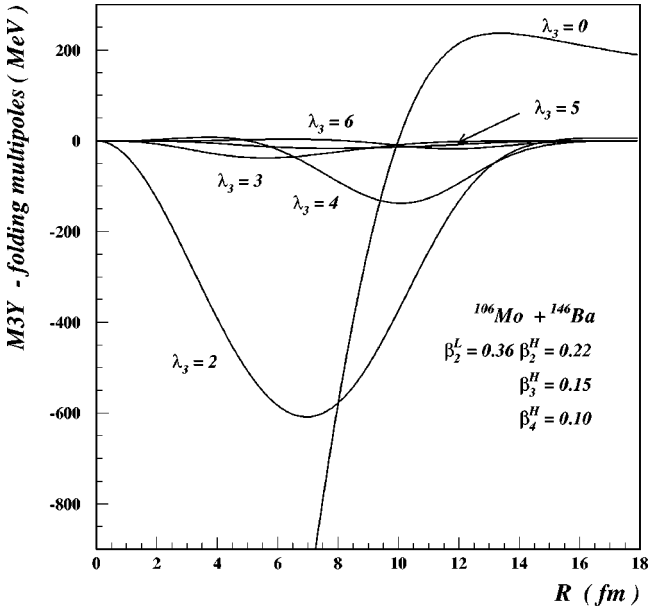

FIG. 3. The influence of the $M3Y$-folding multipoles on the barrier between ^{106}Mo and ^{146}Ba. Notice that the main effect is due to $\lambda_3=2$. The influence of $\lambda_3=3$ is large but less important in the barrier region compared with the induced deformations $\lambda_3=5$ and $\lambda_3=6$.

hexadecupole one. Next, in Fig. 4 we are illustrating for the same partners the cumulative effect of high rank multipoles on the barrier.

III. COLD FISSION BINARY ISOTOPIC YIELDS

We should like to stress again that in our simple cluster model the preformation factors for different channels are neglected, i.e., we use the same assault frequency factor ν for the collisions with the fission barrier for all fragmentations.

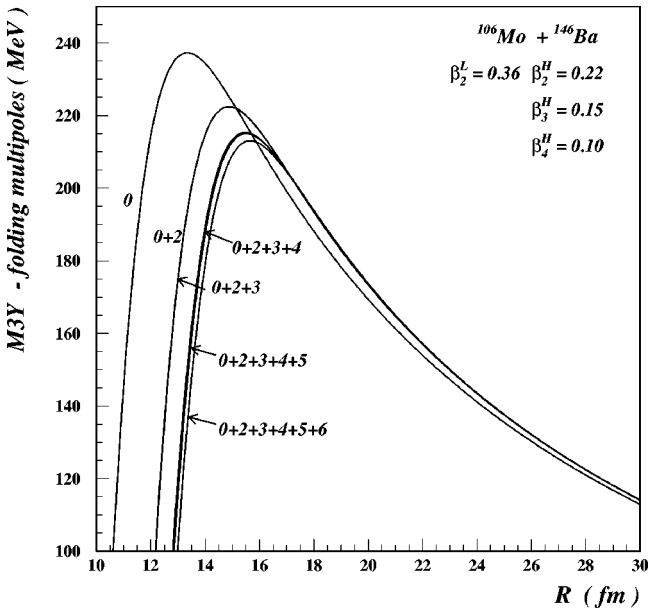

FIG. 4. The cumulative effect of high rank multipoles on the barrier between ^{106}Mo and ^{146}Ba. We considered the deformations β_3 and β_4 to be much larger than the real ones in order to illustrate the effect of deformations.

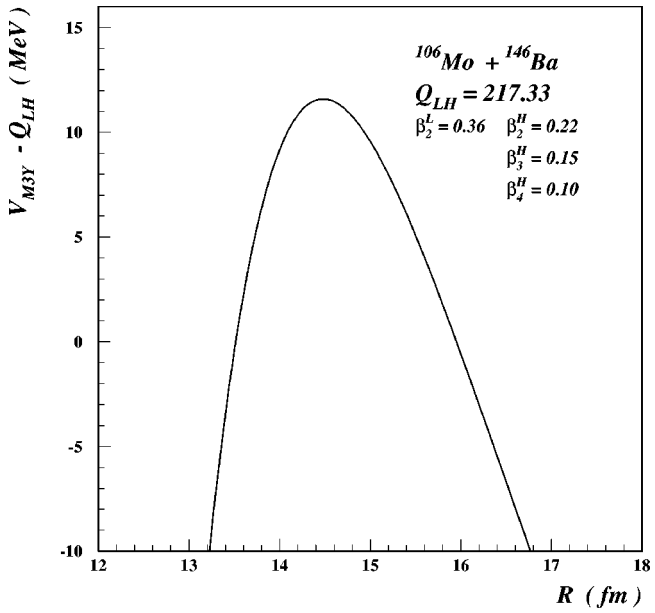

FIG. 5. The barrier between ^{146}Ba and ^{106}Mo as a function of the distance R_{HL} between their centers of mass. By Q_{LH} we denote the decay energy.

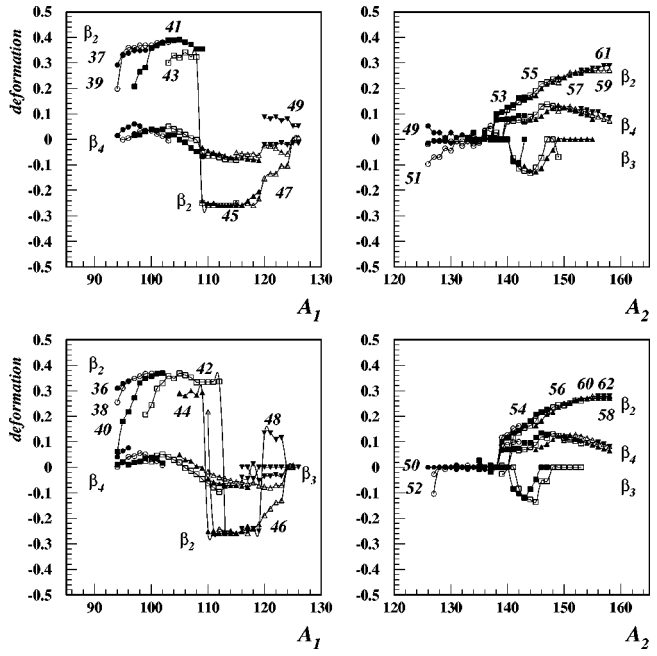

FIG. 6. The assumed β_2, β_3, β_4 ground-state fragment deformations [18]. We can see that the light fragments (Z_1,A_1) have mainly quadrupole deformations in contrast to the heavy fragments (Z_2,A_2). The octupole deformations are existing in a small mass region $141 \leqslant A_2 \leqslant 148$ whereas the hexadecupole deformations are important in the region $138 \leqslant A_2 \leqslant 158$. The fragments with masses $A_1 \leqslant 94$ and $A_2 \leqslant 138$ are practically spherical.

It is generally known that the general trends in α decay of heavy nuclei are very well described by barrier penetrabilities, the preformation factors becoming increasingly important only in the vicinity of the double magic nucleus ^{208}Pb. On the other hand, the cold binary fragmentation of ^{252}Cf was also reasonably well described using constant preformation factors [9,20]. However in this case too, as we shall see later, around the double-magic nucleus ^{132}Sn the preformation turn out to be of capital importance. Eventually, as the experimental data become more accurate we would be able to extract some fragment preformation factors and discuss the related nuclear structure effects.

In the laboratory frame of reference the z axis was taken as the initial fissioning axis of the two fragments, with the origin at their point of contact. The potential barriers $V_F - Q_{LH}$ between the two fragments are high but rather thin with a width of about 2 to 3 fm. As an illustration, we show in Fig. 5 a typical barrier between ^{146}Ba and ^{106}Mo, as a function of the distance R_{LH} between their center of mass. Here Q_{LH} is the decay energy for the binary fragmentation of ^{252}Cf. For the two fragments, the exit point from their potential barrier is at R_{LH} typically between 16 and 17 fm (see Fig. 5) which supports our cluster model.

The penetrabilities through the double-folded potential barrier between the two fragments were calculated by using the WKB approximation

$$P = \exp\left\{ -\frac{2}{\hbar} \int_{s_i}^{s_o} \sqrt{2\mu[V_F(s) - Q_{LH}]}\, ds \right\}, \tag{8}$$

where s is the relative distance, μ is the reduced mass, and s_i and s_o are the inner and outer turning points, defined by $V_F(s_i) = V_F(s_o) = Q_{LH}$. The barriers were computed with the LDM parameters $a_p = a_n = 0.5$ fm, $r_{0p} = r_{0n} = (R - 1/R)A^{-1/3}$ fm with $R = 1.28A^{1/3} + 0.8A^{-1/3} - 0.76$.

Accurate knowledge of Q values is crucial for the calculation, since the WKB penetrabilities are very sensitive to them. We obtained the Q values from experimental mass tables [21], and for some fragmentations the nuclear masses were taken from the extended tables of Möller *et al.* [18] computed using a macroscopic-microscopic model.

Let us consider for the beginning only the relative isotopic yields corresponding to true cold (neutronless) binary fragmentations in which all final nuclei are left in their ground state. These relative isotopic yields are given by the expression $(A_1 = A_L, A_2 = A_H)$

$$Y(A_1,Z_1) = \frac{P(A_1,Z_1)}{\Sigma_{A_1 Z_1} P(A_1,Z_1)}. \tag{9}$$

As we mentioned above the fragment deformations were chosen to be the ground state deformations of Möller *et al.* [18], computed in the frame of the macroscopic-microscopic model. In Fig. 6 we represented separately these deformations for the light A_L and heavy A_H fragments for odd and even charge Z. We can see that the light fragments have mainly quadrupole deformations in contrast to the heavy fragments, which have all types of deformations. The octupole deformations are nonzero in a small heavy fragment mass number region $141 \leqslant A_H \leqslant 148$. The fragments with mass number $A_L \leqslant 92$ and $A_H \leqslant 138$ are practically spherical.

The computed $M3Y$-fission barrier heights, for different assumptions: no deformations, including the quadrupole ones, including the quadrupole and octupole ones and for all deformations, together with the corresponding Q values, are represented in Fig. 7 for odd Z and even Z separately. We

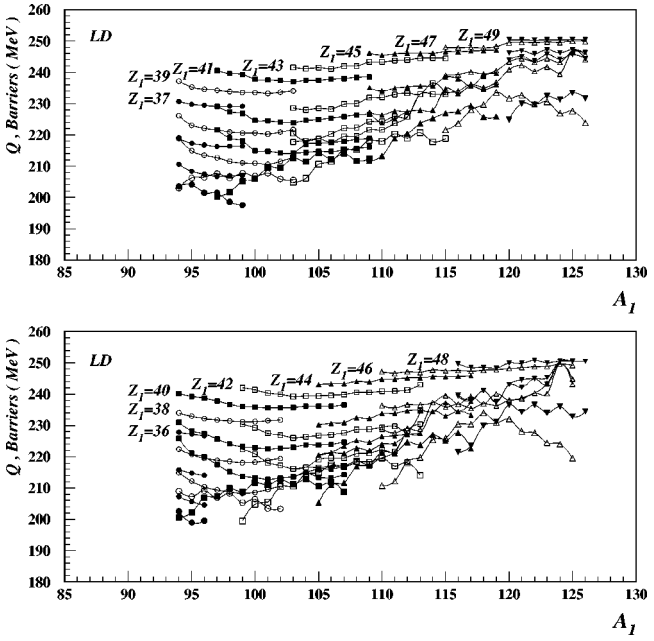

FIG. 7. The barrier heights for all considered fragmentation channels represented for different charges Z_1 and mass numbers A_1 of the light fragment.

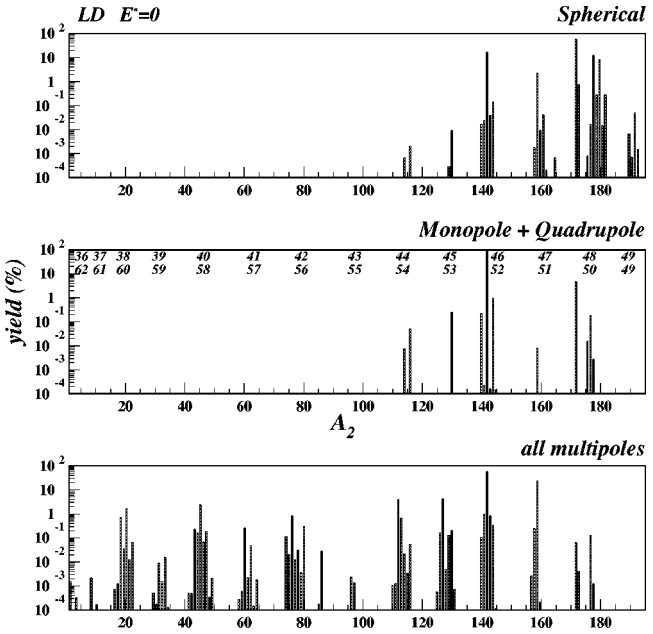

FIG. 8. The true cold fission yields in percent for all fragmentation channels computed with the LDM parameters, for spherical nuclei, with the inclusion of quadrupole deformations and with all deformations at zero excitation energy.

notice the large influence due to the quadrupole deformations but also the hexadecupole ones are lowering the barriers very much. The octupole deformations in the mass region $141 \leqslant A_H \leqslant 148$ have a smaller effect as we expected. This is a illustration of the difference between cluster radioactivity, which is due only to the large Q values and the cold fission which is due mainly to the lowering of the barriers due to the fragment deformations. Both processes are cold fragmentation phenomena.

The computed yields in percent, for the splittings represented by their fragment deformation parameters in Fig. 6 or by their barrier heights in Fig. 7, are given in Fig. 8 for spherical fragments ($\beta_i = 0$), for quadrupole deformations (β_2), and for all deformations ($\beta_2 + \beta_3 + \beta_4$) at zero excitation energy. We can see that when the fragments are assumed to be spherical the splittings with the highest Q values, which correspond to real spherical heavy fragments (see Fig. 6), i.e., for charge combinations $Z_1/Z_2 =$ 48/50, 47/51, and 46/52 are the predominant ones. As we mentioned before this situation is similar to the cluster radioactivity where the governing principle is the Q value. Due to the staggering of Q values (see Fig. 7) the highest yields are for even-even splittings. By including the β_2 deformations a few asymmetric splittings exists. For all deformations more asymmetric yields appear. Now the principal yields are for $Z_1/Z_2 = 38/60$, 40/58, 41/57, and 42/56 along with 44/54, 46/52, and 47/51. This is due to the fact that the influence of the fragment deformations on the yields overcome the influence of Q values in the more asymmetric region. This illustrates the fact that cold fission is a cold rearrangement process in which all deformations are playing the main role and not the Q values. The staggering for odd Z fragmentations like $Z_1/Z_2 = 39/59$, 41/57, 43/55, 45/53, and 47/51 or odd N fragmentations is recognized at first glance. However, by the introduction of the density levels this staggering is reversed. The largest yields will be for odd Z and/or N fragmentations.

In the next figure we represented the mass yields $Y_{A_2} = \Sigma_{Z_2} Y(A_2, Z_2)$ (Fig. 9) for spherical fragments ($\beta_i = 0$), for quadrupole deformations ($\beta_2 \neq 0$) and for all deformations ($\beta_i \neq 0$). We can see in the spherical case that the main mass yields are centered around $A_2 = 132$. All these heavy frag-

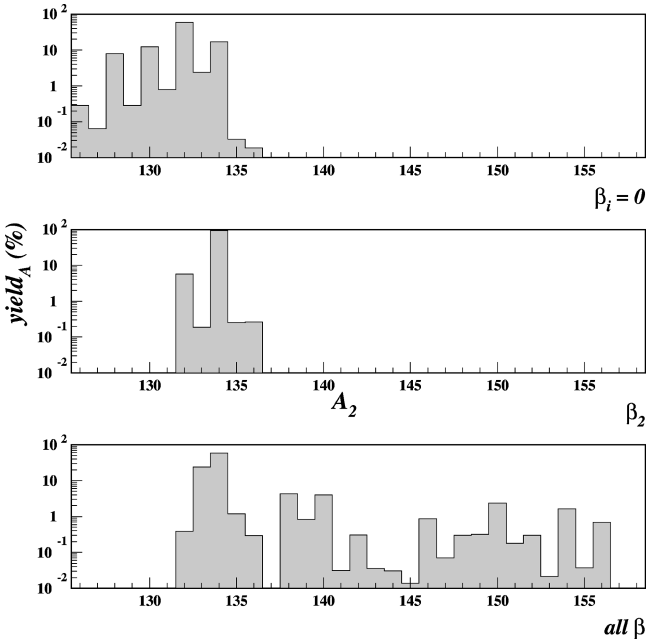

FIG. 9. The mass yields $Y_{A_2} = \Sigma_{Z_2} Y(A_2, Z_2)$ in percent, as a function of light fragment mass computed with LDM parameters. Calculations without deformations ($\beta_{2,3,4} = 0$) enhance only the spherical region $A_2 \leqslant 136$; the inclusion of quadrupole deformations ($\beta_2 \neq 0$) enhances the yield with $A_2 = 134$; for all deformations there are two main mass yields regions, i.e., $133 \leqslant A_2 \leqslant 136$ and $138 \leqslant A_2 \leqslant 156$.

ments are spherical or nearly spherical (with a small prolate deformation) and have high-Q values. Since other spherical fragments do not arise in the yield diagram, it occurs that in the spherical case the Q value is the dictating principle. When we turn on the quadrupole deformation a rearrangement in this spherical region takes place. The yield corresponding to $A_2=132$ is still important but the one for $A_2=134$ takes over, although the maximum decay energy of the first mass split $Q_{\max}$ is larger than that of the former. In this case the larger quadrupole deformation of the light partner decides the augmentation of the $A_2=134$ yield. When we include the higher multipole deformations, i.e., octupole and hexadecupole deformations the yield diagram will change drastically over the whole mass range. First of all, in the spherical region the mass splittings yields $A_2=132$, 134 are lowered whereas their odd neighbors are augmented. Once again this is a consequence of the fact that the hexadecupole deformations of the odd light partners are slightly larger. But the most important change occurs in the mass region $A_2=138-156$ where a whole bunch of splittings show up with yields greater than 0.01%. This is, beyond any doubt, an effect due to the hexadecupole deformations. As can be infered from Fig. 6 the above-mentioned mass region is characterized by noticeable values of the hexadecupole deformation. Before adding the hexadecupole deformation this region was completely desertic, whereas after the inclusion of β_4 the most pronounced peaks are $A_2=138$, 140, 146, 150, and 154. It is the place to mention that the first mass region, in the cold fission of ^{252}Cf reported in the paper of Gönnenwein *et al.* [16] coincides with the range obtained by us employing a deformation-dependent cluster model. However in order to reproduce completely the experimental data we have to underline the elements that have to be supplied further in our model. First, in the spherical region, the experiment claims a mass region of cold fission centered around $A_2=132$, instead of $A_2=134$ as we obtained. However this misfit was to be expected since as we mentioned in the beginning of our paper we did not include the preformation factors. In the case of the doubly magic nucleus ^{132}Sn this assumption proves to be unsatisfactory. As has been advocated by the Tübingen group [16] this is a possible manifestation of heavy-cluster decay. Therefore it is very likely that in this case the preformation factor, which multiplies the penetrability, is larger than for the neighboring nuclei, which could then account for the discrepancies between our calculations and experimental data. However, an encouraging experimental point which supports our calculations is the fact that the even masses 134 and 136 are accompanying the leading yield for 132. In Fig. 10 we compare the total yields for 132 (left side) and 134 (right side). We see that the Z splitting corresponding to the spherical ^{134}Te dominates in all the three cases, because, as we mentioned earlier its light partner has a sensitive quadrupole deformation and a nonvanishing hexadecupole one. Its Z partner ^{134}Sn has a smaller hexadecupole deformation. The same reasoning applies to $A_2=136$. Therefore it could be possible that in the case of these nuclei the deformation dictates the yield magnitude rather than the magic number in protons or neutrons. The experimental determination of the double fine structure in this region will, hopefully, clarify the situation.

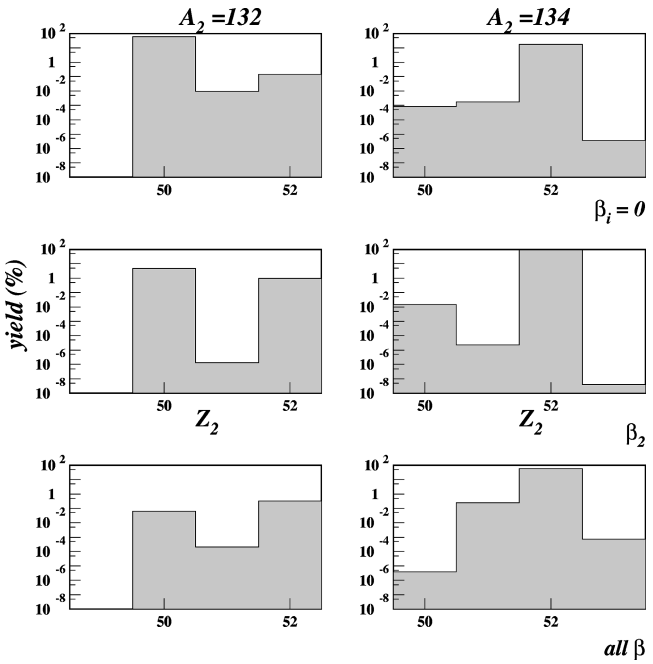

FIG. 10. The yields for the Z splittings of $A_2=132$, 134 in percent computed with LDM parameters.

The *hexadecupole deformed* region, extending from 138 to 156, obtained in the frame of our cluster model, presents also some discrepancies compared to the experimental findings. The main problem that we faced here concerns the odd-even effect which seems to be very strong in this region according to the Tübingen group [15]. This can be understood as follows: In the vicinity of the ground state, the level densities of odd mass nuclei are much larger than for even nuclei and consequently it will be more probable to observe cold fission for odd-odd mass splits in comparison to even-even mass splits. Since in our present calculations the level density of fragments is not taken into account our results points to an enhancement of even-even mass splits with respect to the odd-odd mass splits. In a preceding paper [13] the effect of level density was incorporated in the calculation of yields by means of the Fermi back-shifted model, valid also for small excitation energies. In order to get a rough idea of how the odd-even effect influence the yields, we simply shift the decay energy by the fictious ground-state position Δ taken from the global analysis of Dilg *et al.* [22], $Q^*=Q-\Delta$. In Fig. 11 we represented the same thing like in Fig. 10 but with the above-mentioned shift in the Q value. It is obvious from the inspection of this figure that except $A_2=138$, the odd splittings take over, in agreement with the experimental data. It is worthwhile to stress once again that in our view the mass region extending from 138 to 156 the hexadecupole deformation is the leading mechanism responsible for the cold fragmentation of ^{252}Cf. The lowering of the barriers due to hexadecupole deformation increase dramatically the penetrabilities and eventually the yields. In Fig. 12 we represented the yields for the Z splittings of $A_2=143$. Comparing the first two cases we see that the yields are almost unsensitive to quadrupole deformation. When the hexadecupole deformation is included the distribution changes, all the yields being shifted uniformly (in the log scale) towards magnitudes four times larger. It is worthwhile

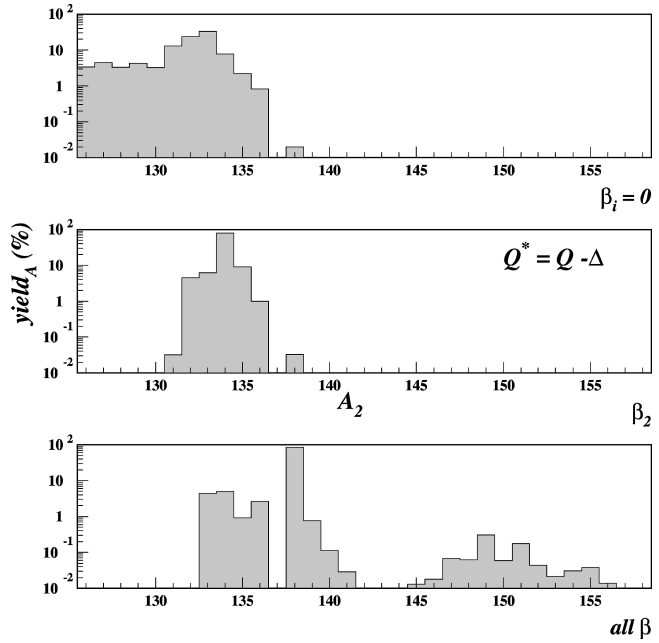

FIG. 11. The mass yields $Y_{A_2}=\Sigma_{Z_2}Y(A_2,Z_2)$ in percent, as a function of light fragment mass computed with LDM parameters with the decay energy modified $Q^*=Q-\Delta$. The odd-odd mass splittings are favored this time.

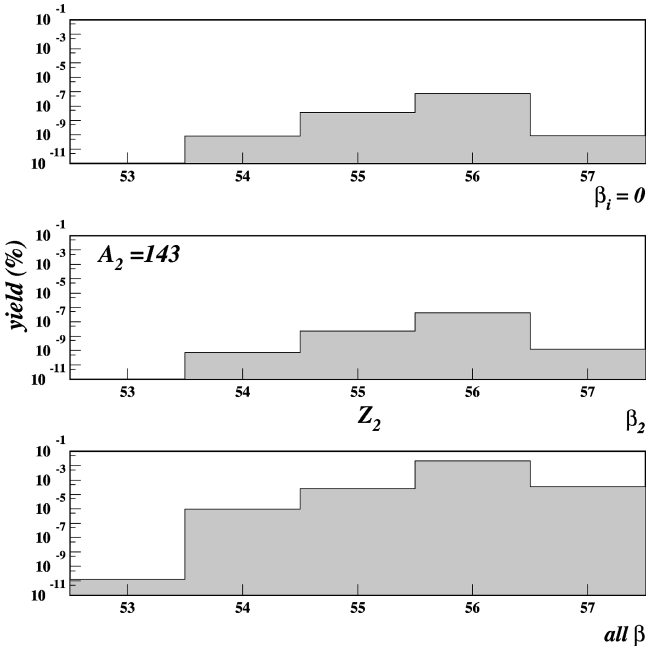

FIG. 12. The yields for the Z splittings of $A_2=143$ in percent computed with LDM parameters. Calculations without deformations and with the inclusion of quadrupole deformation give nearly the same yields. The inclusion of hexadecupole deformation increases uniformly by four orders of the magnitude yields.

to notice before ending this section that the octupole deformations are not inducing the tremendous changes that the hexadecupole do.

IV. DISCUSSIONS AND CONCLUSIONS

The deformation-dependent cluster model which we used in this paper for calculating the isotopic yields associated with cold binary fission, predicts a large number of favored binary splittings in which one or both fragments are well deformed in their ground states. For cold binary fission the initial scission configurations are known: the fragment deformations should be essentially those of the ground-state deformations.

The main result obtained in our paper represents the theoretical confirmation of the existence of two distinct regions of ^{252}Cf cold fission. The results indicate two different mechanisms. In the heavy-mass region situated between 138 and 156, the hexadecupole deformation gives rise to a large number of splittings. Here the shell closure in neutrons or protons seems to not be involved. Although the shell effects should play an important role in the odd-even differences by enhancing the odd-odd mass splits with respect to the even-even one, our results emphasize that the fragments are emitted with the deformations corresponding to those of the ground state. In the spherical region our results give only a hint of the importance of the magic nucleus ^{132}Sn which is susceptible to be produced in a heavy clusterization process, similar to that for light clusters [23]. Here the decay mechanism should be similar to the light cluster radioactivity, the daughter nucleus ^{132}Sn being traded for ^{208}Pb and the heavy cluster ^{120}Cd for ^{14}C.

The results reported in this paper point to the importance of deformations included in the cold fission model, since the Q value seems to be no longer the absolute ruler of the process, as in the case of cluster radioactivity. In the future the investigations should be extended in such a way to explain also the yields structure at finite excitation energy.

[1] J.C.D. Milton and J.S. Fraser, Can. J. Phys. **40**, 1626 (1962).
[2] C. Guet, M. Ashgar, P. Perrin, and C. Signarbieux, Nucl. Instrum. Methods **150**, 189 (1978).
[3] F. Gönnenwein and B. Borsig, Nucl. Phys. **A530**, 27 (1991).
[4] F.-J. Hambsch, H.-H. Knitter, and C. Budtz-Jorgensen, Nucl. Phys. **A554**, 209 (1993).
[5] A. Benoufella, G. Barreau, M. Asghar, P. Audouard, F. Brisard, T.P. Doan, M. Hussonnois, B. Leroux, J. Trochon, and M.S. Moore, Nucl. Phys. **A565**, 563 (1993).
[6] W. Schwab, H.-G. Clerc, M. Mutterer, J.P. Theobald, and H. Faust, Nucl. Phys. **A577**, 674 (1994).
[7] J.H. Hamilton *et al.*, J. Phys. G **20**, L85 (1994).
[8] G.M. Ter-Akopian *et al.*, Phys. Rev. Lett. **73**, 1477 (1994).
[9] A. Săndulescu, A. Florescu, F. Cârstoiu, W. Greiner, J.H. Hamilton, A.V. Ramayya, and B.R.S. Babu, Phys. Rev. C **54**, 258 (1996).
[10] A. Săndulescu and W. Greiner, Rep. Prog. Phys. **55**, 1423 (1992).
[11] A. Săndulescu, A. Florescu, and W. Greiner, J. Phys. G **15**, 1815 (1989).

[12] A.V. Ramayya *et al.*, *Third International Conference on Dynamical Aspects of Nuclear Fission*, 1996, Casta−Papiernicka, Slovak Republic.
[13] A. Săndulescu, F. Cârstoiu, Ş. Mişicu, A. Florescu, A.V. Ramayya, J.H. Hamilton, and W. Greiner, J. Phys. G **24**, 181 (1998).
[14] A.V. Ramayya *et al.*, this issue, Phys. Rev. C **57**, 2370 (1998).
[15] A. Möller, M. Crönni, F. Gönnenwein, and G. Petrov, International Conference on Large Scale Collective Motion of Atomic Nuclei, Brolo, 1996.
[16] F. Gönnenwein, A. Möller, M. Crönni, M. Hesse, M. Wösteinrich, H. Faust, G. Fioni, and S. Oberstedt, Nuovo Cimento (in press).
[17] M.E. Brandan and G.R. Satchler, Phys. Rep. **285**, 143 (1997).
[18] P. Möller, J.R. Nix, W.D. Myers, and W.J. Swiatecki, At. Data Nucl. Data Tables **59**, 185 (1995).
[19] F. Cârstoiu and R.J. Lombard, Ann. Phys. (N.Y.) **217**, 279 (1992).
[20] A. Florescu, A. Săndulescu, C. Cioacă, and W. Greiner, J. Phys. G **19**, 669 (1993).
[21] A.H. Wapstra, G. Audi, and R. Hoeckstra, At. Data Nucl. Data Tables **39**, 281 (1988).
[22] W. Dilg, W. Schantl, H. Vonach, and M. Uhl, Nucl. Phys. **A217**, 269 (1973).
[23] A. Săndulescu and W. Greiner, J. Phys. G **3**, L189 (1977).